Complete Kinetic Mechanism of Homoisocitrate Dehydrogenase from *Saccharomyces cerevisiae*†

Ying Lin, Susan S. Alguindigue, Jerome Volkman, Kenneth M. Nicholas, Ann H. West, and Paul F. Cook*

Department of Chemistry and Biochemistry, University of Oklahoma, 620 Parrington Oval, Norman, Oklahoma 73019

Received October 4, 2006

ABSTRACT: The kinetic mechanism of homoisocitrate dehydrogenase from *Saccharomyces cerevisiae* was determined using initial velocity studies in the absence and presence of product and dead end inhibitors in both reaction directions. Data suggest a steady state random kinetic mechanism. The dissociation constant of the Mg−homoisocitrate complex (MgHIc) was estimated to be 11 ± 2 mM as measured using Mg^{2+} as a shift reagent. Initial velocity data indicate the MgHIc complex is the reactant in the direction of oxidative decarboxylation, while in the reverse reaction direction, the enzyme likely binds uncomplexed Mg^{2+} and α-ketoadipate. Curvature is observed in the double-reciprocal plots for product inhibition by NADH and the dead-end inhibition by 3-acetylpyridine adenine dinucleotide phosphate when MgHIc is the varied substrate. At low concentrations of MgHIc, the inhibition by both nucleotides is competitive, but as the MgHIc concentration increases, the inhibition changes to uncompetitive, consistent with a steady state random mechanism with preferred binding of MgHIc before NAD. Release of product is preferred and ordered with respect to CO_2, α-ketoadipate, and NADH. Isocitrate is a slow substrate with a rate (V/E_t) 216-fold slower than that measured with HIc. In contrast to HIc, the uncomplexed form of isocitrate and Mg^{2+} bind to the enzyme. The kinetic mechanism in the direction of oxidative decarboxylation of isocitrate, on the basis of initial velocity studies in the absence and presence of dead-end inhibitors, suggests random addition of NAD and isocitrate with Mg^{2+} binding before isocitrate in rapid equilibrium, and the mechanism approximates rapid equilibrium random. The K_{eq} for the overall reaction measured directly using the change in NADH as a probe is 0.45 M.

Homoisocitrate dehydrogenase (3-carboxy-2-hydroxyadipate dehydrogenase, EC 1.1.1.87) (HIcDH)[1] catalyzes the fourth reaction of the α-aminoadipate pathway (AAA) for lysine synthesis, the NAD-dependent conversion of homoisocitrate to α-ketoadipate (α-Ka) (Scheme 1) (*1*). Among the 20 common proteinogenic amino acids, lysine is the only one known to have two diverse pathways for its synthesis (*2*). In bacteria, plants, and lower fungi such as phycomycetes or algal fungi, lysine is synthesized via the diaminopimelate pathway, beginning with the phosphorylation of aspartate by aspartokinase. However, it is synthesized via the α-aminoadipate pathway in euglenoids and higher fungi such as *Saccharomyces cerevisiae* and human pathogenic fungi such as *Candida albicans*, *Cryptococcus neoformas*, and *Aspergillus fumigatus*, and plant pathogens like *Magnaporthe grisea* use this pathway (*2*−*4*). The uniqueness of the α-aminoadipate pathway makes it a potential target for new antifungal drugs (*5*).

Scheme 1: Reaction Catalyzed by HIcDH

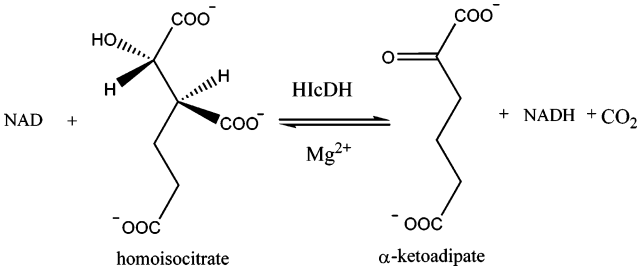

HIcDH is a member of the family of pyridine nucleotide-dependent β-hydroxyacid oxidative decarboxylases which includes, among others, ICDH, IPMDH, malic enzyme, TDH, and 6-PGDH. The reactions catalyzed by these enzymes are essentially equivalent (*6*). With the exception of 6-PGDH which is metal ion-independent, all of the enzymes require a divalent metal ion activator. The NAD-specific ICDH selectively binds the Mn−isocitrate chelate complex where Mn^{2+} is coordinated to the α-hydroxyl and α-carboxylate of threo-D_s isocitrate (*7*). NAD-Malic enzyme and IPMDH bind the uncomplexed forms of the metal ion

† This work is supported by National Institutes of Health Grant GM 071417 (to P.F.C. and A.H.W.) and the Grayce B. Kerr Endowment to the University of Oklahoma (to P.F.C.).

* To whom correspondence should be addressed. E-mail: pcook@chemdept.chem.ou.edu. Telephone: (405) 325-4581. Fax: (405) 325-7182.

[1] Abbreviations: HIcDH, homoisocitrate dehydrogenase; AAA, α-aminoadipate pathway; 6-PGDH, 6-phosphogluconate dehydrogenase; ICDH, isocitrate dehydrogenase; IPMDH, 3-isopropylmalate dehydrogenase; TDH, tartrate dehydrogenase; NAD, nicotinamide adenine dinucleotide (the positive charge on the nicotinamide ring is omitted for convenience); NADH, reduced nicotinamide adenine dinucleotide; α-Ka, α-ketoadipate; HIc, homoisocitrate; MgHIc, Mg^{2+}−homoisocitrate complex; Hepes, 4-(2-hydroxyethyl)-1-piperazineethanesulfonic acid; IPTG, isopropyl β-D-thiogalactopyranoside; LB, Luria-Bertani; β-ME, mercaptoethanol; 3-AcPyADP, 3-acetylpyridine adenine dinucleotide phosphate; C, competitive inhibition; NC, noncompetitive inhibition; UC, uncompetitive inhibition; Ni-NTA, nickel-nitrilotriacetic acid.

10.1021/bi062067q CCC: $37.00
Published on Web 12/22/2006

and substrate (*8*, *9*). In general, the overall kinetic mechanisms of the enzymes that have been studied in detail are random; enzymes include the NAD-malic enzyme from *Ascaris suum* (*9*, *10*), the NADP malic enzyme from chicken liver (*11*), the NADP-dependent ICDH from pig heart (*12*, *13*) and *Escherichia coli* (*14*), 6-PGDH from *Candida utilis* (*15*) and sheep liver (*16*), IPMDH from *Thermus thermophilus* (*8*), and TDH from *Pseudomonas putida* (*17*). With the exception of 6-PGDH, which has a rapid equilibrium random kinetic mechanism, all have a steady state random kinetic mechanism. In the case of HIcDH, the reported K_m values for homoisocitrate and NAD are 10 μM and 0.33 mM, respectively, and the enzyme has a pH optimum of ~8.5 in the direction of oxidative decarboxylation of homoisocitrate and ~7.0 in the direction of reductive carboxylation of α-Ka (*2*). Nothing about the mechanism of this enzyme is known.

In this paper, we use initial velocity studies in the absence and presence of product and dead-end inhibitors to elucidate the overall kinetic mechanism of HIcDH from *S. cerevisiae*. Data are also used to estimate the equilibrium constant using the Haldane relationship, which is compared to the value obtained directly. The kinetic mechanism for the slow substrate, isocitrate, has also been studied and compared with that using homoisocitrate (HIc).

MATERIALS AND METHODS

Chemicals. Isocitrate, citrate, oxalate, and 3-AcPyADP were obtained from Sigma. β-NADH, β-NAD, LB broth, and LB agar were purchased from USB. The nickel-nitrilotriacetic acid (Ni-NTA) agarose resin was from Qiagen. Isopropyl β-D-thiogalactopyranoside (IPTG), *Nde*I, *Xho*I, Turbo Pfu polymerase, and T4 DNA ligase were from Invitrogen. Ampicillin was from Fisher Biotech, and Hepes was from Research Organics. Homoisocitrate was the generous gift of D. R. J. Palmer (University of Saskatchewan, Saskatoon, SK).

α-Ketoadipate was prepared according to a published procedure (*18*). The Claisen condensation of diethyl glutarate with diethyl oxalate gave a 67% yield of ethyl α-oxalylglutarate, which was treated with concentrated hydrochloride acid to obtain α-Ka in 71% yield. The melting point of the final α-Ka product was 120−124 °C. Data from ^{1}H NMR (300 MHz) in acetone-d_6 gave the following δ values in parts per million: 1.88 [p, J = 7.5 Hz, 2H, C(4)-H_2], 2.39 [t, J = 7.5 Hz, 2H, C(5)-H_2], 2.98 [t, J = 7.5 Hz, 2H, C(3)-H_2], 10.8 (bs, COOH). ^{13}C (75.5 MHz, $CDCl_3$) gave δ values of 195.9 (C2), 174.6 (C6), 162.2 (C1), 38.2 (C3), 32.9 (C5), and 19.0 (C4).

Molecular Cloning, Cell Growth, and Protein Expression. Two primers, 5′-GGACTCCCATATGTTAGATCTGTTGCTACTAG-3′ and 5′-CCGCTCGAGCTTCTATAATCTCGACAAAACGTCG-3′, were designed for PCR to produce a DNA fragment corresponding to the *Lys 12* gene encoding HIcDH from *S. cerevesiae*. The first primer introduced an *Nde*I restriction site (underlined), while the second one introduced an *Xho*I restriction site. A 1116 bp fragment was amplified by PCR using yeast genomic DNA as the template via the following protocol: one cycle of initial denaturation at 95 °C for 4 min, followed by 45 cycles of denaturation at 95 °C for 1 min, annealing at 60 °C for 1 min, and extension at 72 °C for 90 s, followed by one cycle of extension at 72 °C for 10 min. Pfu polymerase, which produces blunt end PCR products, was used. The amplified DNA fragment was digested with *Nde*I and *Xho*I restriction endonucleases and subcloned into the similarly digested pET16b vector which adds a 10-His tag to the N-terminal end of the protein. The sequence of the cloned gene was confirmed by DNA sequencing carried out by the Laboratory for Genomics and Bioinformatics of the University of Oklahoma Health Sciences Center (Oklahoma City, OK). The plasmid was used to transform *E. coli* BL21*DE3 or BL21*DE3 RIL competent cells, which were grown in LB medium at 25 °C, with gentle shaking until the OD reached ~0.6. IPTG was added to a concentration of 1 mM, and after a 5 h induction period, the cells were harvested by centrifugation at 4500*g*. Cells were then lysed in extraction buffer [20 mM Tris-HCl, 500 mM NaCl, 10 mM $MgCl_2$, and 2 mM β-ME (pH 7.5)] by sonication on ice using a MISONIX Sonicator XL device for 5 min (a 15 s pulse followed by a 15 s rest). The cell extract was loaded onto a 5.5 cm × 2 cm Ni-NTA column equilibrated with 20 mM Tris-HCl, 500 mM NaCl, 10 mM $MgCl_2$, and 2 mM β-ME (pH 7.5). The same buffer containing imidazole at concentrations of 20, 30, 90, 120, 150, 200, 300, and 500 mM was then used to elute the enzyme. The HIcDH eluted at 150−200 mM imidazole. The enzyme solution was maintained at −80 °C in the elution buffer with 10% glycerol.

Enzyme Assay. The reaction was followed by assessing the appearance or disappearance of NADH at 340 nm (ϵ = 6220 M^{-1} cm^{-1}) using a Beckman DU 640 spectrophotometer. All assays were carried out at 25 °C, and the temperature was maintained with a Neslab RTE-111 circulating water bath. A unit of enzyme activity is defined as the amount of enzyme catalyzing the production or utilization of 1 μmol of NADH/min at 25 °C.

In the direction of oxidative decarboxylation of HIc (forward reaction), rate measurements were carried out in 0.5 mL of 50 mM Hepes (pH 7.5). Reactions were initiated by addition of 5 μL of an appropriately diluted enzyme solution to a mixture that contained all other reaction components, and the initial linear portion of the time course was used to calculate the initial velocity. Since the diluted enzyme solution (protein concentration of ~150 μg/mL) is not stable when kept on ice for approximately half a day, it was prepared fresh daily. In the direction of reductive carboxylation of α-Ka (reverse reaction), rate measurements were carried out in 0.5 mL of 1 M Hepes (pH 7.0). The reactions were initiated by adding 5 μL of enzyme solution (protein concentration of ~1.5 mg/mL). With isocitrate used as a substrate, reactions were initiated by adding 50 μL of enzyme solution (protein concentration of ~1.5 mg/mL), and all other conditions are as for assays with HIc.

Determination of the Dissociation Constant of the Mg−HIc Complex by ^{1}H NMR. The dissociation constant of the Mg−HIc chelate complex was determined by ^{1}H NMR using Mg^{2+} as a shift reagent. A solution in D_2O of 10 mM HIc at pD 7.7 was prepared. Different concentrations of $MgSO_4$ (0, 5, 10, 50, 100, 200, 300, and 500 mM) were added to the HIc solution. All NMR experiments were performed on a Varian Mercury VX-300 MHz spectrometer with a Varian four-nucleus auto-switchable PFG probe. ^{1}H NMR spectra were collected using the PRESAT pulse sequence supplied

by Varian Inc. The spectra were collected with a sweep width of 4803.1 Hz and 16 transients.

^{1}H NMR referenced to HDO (4.68 ppm) and collected at pH 7 and 21 °C with no added Mg^{2+} gave δ values of 3.82 [d, 1H, C(2)-H], 2.31 [dd, 1H, C(3)-H], 2.03 [t, 2H, C(5)-H_2], and 1.61 [m, 2H, C(4)-H_2]. As Mg^{2+} was added, the resonance at 3.8 ppm [reflecting C(2)-H] of HIc exhibited the biggest shift, as expected. The Mg^{2+} dependence of the change in chemical shift was fitted using eq 1 to estimate the K_d.

$$y = \frac{(y_{max})x}{K_d + x} \quad (1)$$

where y is the chemical shift change, x is the Mg^{2+} concentration, and y_{max} is the maximum chemical shift change.

Initial Velocity Studies. Systematic Analysis. In the direction of α-Ka formation, the initial rate was measured as a function of NAD concentration (0.2, 0.3, 0.5, and 2 mM) at different fixed concentrations of HIc (15, 30, 50, and 150 μM) and a fixed concentration of $MgCl_2$ (0.5 mM). The experiment was then repeated at several additional $MgCl_2$ concentrations (1, 2, and 5 mM). Once it was determined that MgHIc is the substrate, initial rate studies were carried out using varying concentrations of MgHIc at different fixed levels of NAD.

Initial velocity studies were also carried out in the direction of reductive carboxylation of α-Ka. In this case, the initial rate was measured as a function of α-Ka concentration (2.5, 5, 10, and 25 mM) at different fixed levels of NADH (0.025, 0.05, 0.1, and 0.2 mM) and fixed concentrations of CO_2 (4 mM) and $MgCl_2$ (20 mM). The experiment was then repeated at several additional CO_2 concentrations (10, 20, and 45 mM). CO_2 was added as $NaHCO_3$, and its concentration was calculated using the Henderson−Hasselbach equation and a pK of 6.1 for H_2CO_3.

With isocitrate as the substrate, the initial rate was measured as a function of NAD concentration (2, 5, 10, and 20 mM) and at different fixed concentrations of isocitrate (1, 2, 5, and 10 mM) and a fixed concentration of $MgCl_2$ (0.5 mM). The experiment was then repeated at several additional $MgCl_2$ concentrations (1, 2, and 5 mM).

Pairwise Analysis. Initial velocities were measured at varying concentrations of one substrate at different fixed concentrations of a second and with the third substrate saturating. For the reaction in the direction of reductive carboxylation of α-Ka, the initial rate was measured as a function of α-Ka at several fixed levels of CO_2 (4, 8, 15, and 45 mM) and with the NADH concentration fixed at 0.8 mM (10 K_m). Because of the high absorbance at 340 nm, data were collected at 363 nm using an ϵ_{363} of 3.11 mM^{-1} cm^{-1}. The rate was also measured as a function of CO_2 concentration at several fixed levels of NADH (0.025, 0.05, 0.1, and 0.2 mM) and with the α-Ka concentration fixed at 60 mM (20K_m). In all cases, the Mg^{2+} concentration was maintained at 20 mM.

Similar experiments were carried out for the isocitrate reaction. For example, the initial rate was measured as a function of isocitrate concentration at several fixed levels of Mg^{2+} (0.5, 1, 2, and 5 mM) and with the NAD concentration at a saturating level (20K_m). For the Mg^{2+}−NAD pair, isocitrate was 20 mM (10K_m).

Product and Dead-End Inhibition Studies. Initial velocity patterns were obtained by measuring the initial rate at different concentrations of one reactant, with the concentration of the other reactants fixed at their respective K_m values, and at different fixed concentrations of the inhibitor, including zero. In all cases, an initial estimate of the K_i for the inhibitor was obtained by fixing the varied substrate at its K_m value and varying the inhibitor concentration. The appK_i was initially estimated by Dixon analysis, a plot of $1/v$ versus I, with all reactants equal to their K_m, extrapolating to $1/v$ equal to zero, and dividing the value of I by 2.

Data Analysis. Initial velocity data were first analyzed graphically using double-reciprocal plots of initial velocity versus substrate concentration and suitable secondary plots. Data were then fitted using the appropriate equation and the Marquardt−Levenberg algorithm supplied with EnzFitter from BIOSOFT (Cambridge, U.K.). Kinetic parameters and their corresponding standard errors were estimated using a simple weighting method.

Data obtained from the systematic analysis for the reaction using MgHIc as a substrate were fitted using eq 2. For the reaction using isocitrate as a substrate, data were fitted using eqs 3 and 4 for a terreactant kinetic mechanism (see the Results and Discussion). For the reverse of the HIc reaction, data were fitted using eqs 3 and 5 for a terreactant kinetic mechanism. For the data sets obtained from a pairwise analysis for the isocitrate reaction, two data sets for the reverse reaction using α-Ka as the substrate were fitted using either eq 2 for a sequential mechanism, eq 6 for an equilibrium ordered mechanism, or eq 7, with the constant term absent. Data conforming to competitive, noncompetitive, or uncompetitive inhibition were fitted using eqs 8−10. Data obtained for oxalate inhibition against HIc or NAD were fitted using eq 11.

$$v = \frac{VAB}{K_{ia}K_b + K_aB + K_bA + AB} \quad (2)$$

$$v = \frac{VABC}{\text{constant} + (\text{coefA})A + (\text{coefB})B + (\text{coefC})C + K_cAB + K_bAC + K_aBC + ABC} \quad (3)$$

$$v = \frac{ABC}{\text{constant} + (\text{coefA})A + 0.2C + K_bAC + K_aBC + ABC} \quad (4)$$

$$v = \frac{VABC}{\text{constant} + (\text{coefA})A + (\text{coefC})C + K_bAC + K_aBC + ABC} \quad (5)$$

$$v = \frac{VAB}{K_{ia}K_b + K_bA + AB} \quad (6)$$

$$v = \frac{VAB}{K_aB + K_bA + AB} \quad (7)$$

$$v = \frac{VA}{K_a\left(1 + \frac{I}{K_{is}}\right) + A} \quad (8)$$

$$v = \frac{VA}{K_a\left(1 + \frac{I}{K_{is}}\right) + A\left(1 + \frac{I}{K_{ii}}\right)} \quad (9)$$

$$v = \frac{VA}{K_a + A\left(1 + \frac{I}{K_{ii}}\right)} \quad (10)$$

$$v = \frac{VA}{K_a\left(1 + \frac{I^2}{K_i^2}\right) + A\left(\frac{1 + I/K_{idenum}}{1 + I/K_{inum}}\right)} \quad (11)$$

where v and V are initial and maximum velocities, respectively, A, B, and C are substrate concentrations, I is inhibitor concentration, and K_a, K_b, and K_c are Michaelis constants for substrates A−C, respectively. In eq 2, K_{ia} is the dissociation constant for dissociation of A from the EA complex. In eqs 3−5, the coef terms are products of kinetic constants that are mechanism-dependent (see the *Discussion*). In eqs 8−10, K_{is} and K_{ii} represent inhibition constants for the slope and intercept, respectively. In eq 11, K_i is the dissociation constant for dissociation of oxalate from the E−oxalate and E−(oxalate)$_2$ complexes, K_{ium} is the dissociation constant for binding of oxalate to the E−NADH product complex, K_{idenum} is a constant that contributes to the hyperbolic nature of the intercept effect, and all the other terms are the same as defined above.

Determination of K_{eq} and the Haldane Relationship for the Reaction Using HIc as a Substrate. In a 500 μL reaction mixture, the concentrations of HIc, NAD, NADH, CO_2, and $MgCl_2$ were fixed at 0.05, 0.01, 0.2, 0.5, and 10 mM, respectively, and the concentration of α-Ka was varied over the range of 0.1−5 mM. The reaction was initiated by the addition of enzyme. The difference in A_{340} representing displacement from equilibrium was plotted against the α-Ka concentration. K_{eq} is obtained using the concentrations given above and the concentration of α-Ka that gave a ΔA_{340} of zero according to eq 12.

$$K_{eq} = \frac{[\text{NADH}][\alpha\text{-Ka}][CO_2]}{[\text{NAD}][\text{MgHIc}]} \quad (12)$$

K_{eq} was also estimated from one of the Haldane relationships for a Bi-Ter kinetic mechanism according eq 13.

$$K_{eq} = \frac{\left(\frac{V_1}{K_{NAD}}\right)K_{iNADH}K_{i\alpha-Ka}}{\left(\frac{V_2}{K_{CO_2}}\right)K_{iMgHIc}} \quad (13)$$

RESULTS

Protein Expression and Purification. HIcDH is eluted from the Ni-NTA column most efficiently with 150−200 mM imidazole, and the purity of the eluted HIcDH is ∼98% as judged by SDS−PAGE. Approximately 2.5 mg of enzyme is obtained per gram of wet cell paste. His-tagged HIcDH is stored with 10% glycerol at −80 °C in elution buffer. The protein is stable under these conditions for more than 1 month.

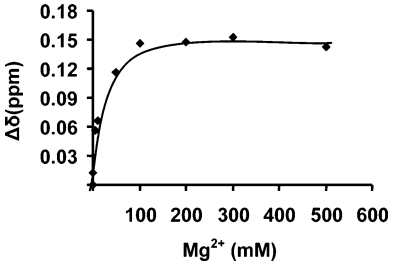

FIGURE 1: Determination of the dissociation constant for MgHIc. The difference in the chemical shift change of the peak at 3.8 ppm (C2 of HIc) from the ^{1}H NMR spectra is plotted vs Mg^{2+} concentration. The points are experimental, while the solid line is theoretical and based on a fit to eq 1.

Determination of the Dissociation Constant of the Mg−HIc Complex by ^{1}H NMR. The chemical shift at 3.8 ppm [reflecting C(2)-H] showed the biggest shift with increasing Mg^{2+} concentration as expected since it is α to one of the coordination positions for Mg^{2+}. A plot of the change in chemical shift versus Mg^{2+} concentration was used to estimate a K_d of 11 ± 2 mM for the Mg−HIc complex (Figure 1).

Identification of the True Substrate in Both Reaction Directions. Since HIcDH requires a divalent metal ion for activity, it is important to determine whether the uncomplexed metal and reactant or the metal−reactant chelate complex is the true substrate. In the direction of reductive carboxylation of α-Ka, an attempt to measure the dissociation constant of the Mg−α-Ka complex by ^{1}H NMR gave no obvious complex formation over the range of 0−3 ppm (data not shown). Therefore, enzyme likely binds the uncomplexed species. During the course of these experiments, it was noted that Mg^{2+} catalyzed the rapid deuteration of α-Ka at C3 as shown by loss of the C3 resonance.

In the direction of oxidative decarboxylation, an initial velocity pattern was obtained by varying the Mg^{2+} concentration at several different fixed levels of HIc with the NAD concentration fixed at 5K_m. Data were then plotted in double-reciprocal form, with $1/v$ plotted versus the concentration of the Mg−HIc complex. If the Mg−HIc complex is the reactant, all 16 points should fall on a straight line, whereas if the uncomplexed species bind to the enzyme, a series of straight lines will be obtained. Data shown in Figure 2 indicate the Mg−HIc complex is the substrate for HIcDH. With isocitrate as the substrate, however, the uncomplexed forms of Mg^{2+} and isocitrate are the true activator and reactant, respectively (data not shown).

Systematic Analysis. The initial velocity was measured at different concentrations of NAD and several different fixed levels of MgHIc. The double-reciprocal plots intersected to the left of the ordinate, suggesting a sequential mechanism (data not shown). Data were fitted to eq 2, and kinetic parameters are summarized in Table 1.

Data were also obtained in the reverse reaction direction at pH 7.0. The initial rate was measured as a function of NADH concentration at different fixed levels of α-Ka and a

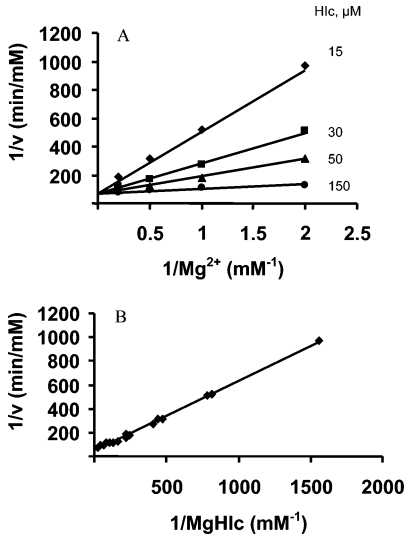

FIGURE 2: MgHIc is the substrate for HIcDH. (A) Double-reciprocal plots obtained upon varying the Mg^{2+} concentration at several different fixed levels of HIc with the NAD concentration fixed at 2 mM. Rates were measured in 50 mM Hepes (pH 7.5) at 25 °C. (B) Double-reciprocal plot with $1/v$ plotted against the MgHIc concentration calculated using the K_d for MgHIc determined from Figure 1.

Table 1: Kinetic Parameters of HIcDH Using Homoisocitrate and Isocitrate as Substrates[a]

Oxidative Decarboxylation of HIc	
K_{NAD} (mM)	0.45 ± 0.08
K_{MgHIc} (mM)	0.0042 ± 0.0009
K_{iMgHIc} (mM)	0.002 ± 0.001
V_1/E_t (s^{-1})	13 ± 1
$V_1/K_{NAD}E_t$ (M^{-1} s^{-1})	$(2.8 \pm 0.2) \times 10^4$
$V_1/K_{MgHIc}E_t$ (M^{-1} s^{-1})	$(3.1 \pm 0.2) \times 10^6$
Reductive Carboxylation of α-Ka	
K_{NADH} (mM)	0.090 ± 0.001
$K_{α-Ka}$ (mM)	3.2 ± 0.1
K_{CO_2} (mM)	16.3 ± 0.3
constant (mM^3)	0.29 ± 0.09
coefA (mM^2)	26 ± 2
V_2/E_t (s^{-1})	2.8 ± 0.2
$V_2/K_{NADH}E_t$ (M^{-1} s^{-1})	$(3.1 \pm 0.2) \times 10^3$
$V_2/K_{α-Ka}E_t$ (M^{-1} s^{-1})	88 ± 5
$V_2/K_{CO_2}E_t$ (M^{-1} s^{-1})	17 ± 3
Oxidative Decarboxylation of Isocitrate	
K_{NAD} (mM)	2.5 ± 0.8
K_{Isoc} (mM)	2.6 ± 0.6
coefA (mM^2)	0.6 ± 0.5
coefC (mM^2)	16 ± 4
constant (mM^3)	35 ± 6
V_1/E_t (s^{-1})	0.062 ± 0.004
$V_1/K_{NAD}E_t$ (M^{-1} s^{-1})	26 ± 2
$V_1/K_{Isoc}E_t$ (M^{-1} s^{-1})	25 ± 2

[a] Data were obtained in the direction of oxidative decarboxylation at pH 7.5 and 25 °C and the direction of reductive carboxylation at pH 7.0 and 25 °C.

fixed concentration of CO_2 (added as HCO_3^-) and Mg^{2+}. The experiment was then repeated at several different levels of CO_2. Estimates of all of the kinetic parameters in this reaction direction were obtained by fitting the data to the equation for a fully random terreactant mechanism (eq 3). The constant term (not possible in a sequential mechanism) and coefB terms were undefined. From a graphical analysis of the data, the values of V and coefC were very well defined. Numeric values of these terms were fixed to generate eq 4,

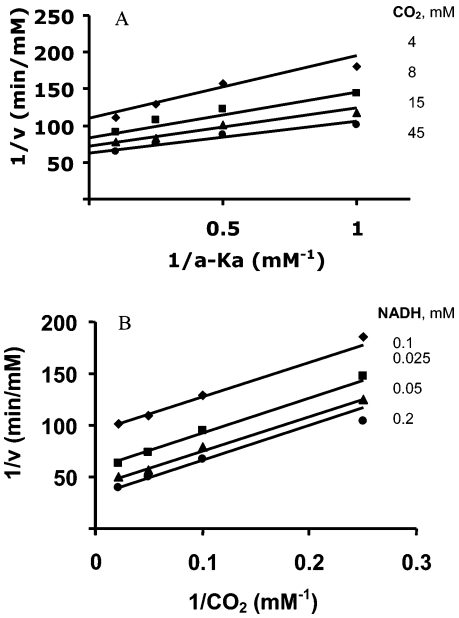

FIGURE 3: Pairwise analysis of the HIcDH reductive carboxylation reaction using MgHIc as the substrate. Double-reciprocal plots obtained when one substrate was varied at different fixed concentrations of a second and with the third substrate at a saturating level. Rates were measured in 50 mM Hepes (pH 7.0) at 25 °C. (A) Initial velocity pattern obtained with the α-Ka−CO_2 pair with NADH at 0.8 mM ($10K_m$). (B) Initial velocity pattern obtained with the NADH−CO_2 pair with the α-Ka concentration at 60 mM ($20K_m$). The points are experimental, while the solid lines are theoretical and based on a fit to eq 2 in panel A and to eq 7 in panel B.

and the data were then fitted to this new equation. Values of the remaining kinetic parameters determined were identical to those obtained using eq 3 and are summarized in Table 1.

Initial velocity patterns were obtained for the reaction using isoctitrate as a substrate and varying the concentrations of NAD and isocitrate at different fixed concentrations of Mg^{2+}. The crossover points for all double-reciprocal plots were to the left of the ordinate (data not shown). All of the initial velocity data were fitted to the equation for a fully random terreactant mechanism (eq 3) to determine which terms in the denominator of the rate equation are absent. The K_c term was undefined, which suggests a kinetic mechanism with rapid equilibrium addition of Mg^{2+}. Kinetic parameters are summarized in Table 1.

Pairwise Analysis. To further define the terreactant kinetic mechanism for the reserve reaction, initial velocity patterns varying one substrate at different fixed concentrations of a second and with the third substrate saturating were obtained and are shown in Figure 3. An intersecting initial velocity pattern was obtained for the α-Ka−CO_2 pair (Figure 3A), while the NADH−CO_2 pair gave a parallel pattern (Figure 3B). These patterns are consistent with several kinetic mechanisms, including a fully ordered one and one that requires ordered addition of NADH, followed by random addition of CO_2 and α-Ka. Kinetic parameters were obtained by fitting the data to eqs 3 and 4. The values of kinetic parameters were in good agreement with those obtained via the systematic analysis discussed above.

To define the terreactant kinetic mechanism for the isocitrate reaction, the same experiments were carried out as for HIc, and the results are shown in Figure 4. The initial

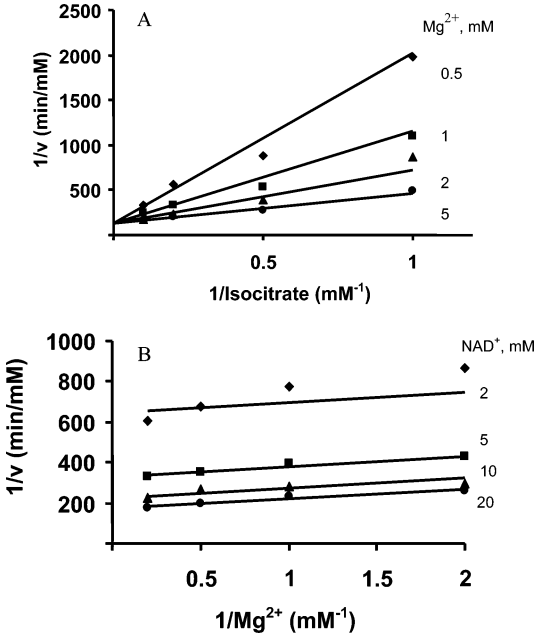

FIGURE 4: Pairwise analysis of the HIcDH oxidative decarboxylation reaction using isocitrate as the substrate. Double-reciprocal plots obtained when one substrate was varied at different fixed concentrations of a second and with the third substrate at a saturating level. Rates were measured in 50 mM Hepes (pH 7.5) at 25 °C. (A) Initial velocity pattern obtained with the isocitrate−Mg^{2+} pair with NAD at 40 mM (20K_m). (B) Initial velocity pattern obtained with the NAD−Mg^{2+} pair with isocitrate at 20 mM (10K_m). The points are experimental, while the solid lines are theoretical and based on a fit to eq 2 in panel A and to eq 7 in panel B.

Table 2: Product Inhibition Patterns for HIcDH with HIc as the Substrate[a]

variable substrate	fixed substrate[b]	inhibitor	K_{is}[c] (mM)	K_{ii}[d] (mM)	pattern
NAD	MgHIc	NADH	0.32 ± 0.05	1.1 ± 0.2	NC
MgHIc (low)	NAD	NADH	0.24 ± 0.03	−	C
MgHIc (high)	NAD	NADH	−	0.35 ± 0.01	UC
NAD	MgHIc	α-Ka	−	7.7 ± 0.5	UC
MgHIc	NAD	α-Ka	−	5.8 ± 0.7	UC

[a] Data were obtained at pH 7.5 and 25 °C. [b] Fixed substrates are maintained at their respective K_m. [c] K_{is} represents the inhibition constant for the slope. [d] K_{ii} represents the inhibition constant for the intercept.

velocity pattern for the isocitrate−Mg^{2+} pair intersects on the ordinate, which indicates equilibrium ordered addition of Mg^{2+} before isocitrate. The Mg^{2+}−NAD pair gave a parallel pattern, suggesting isocitrate adds between NAD and Mg^{2+}. On the basis of these results, data from double-reciprocal initial velocity studies were then fitted to eqs 3 and 5, and values of the kinetic parameters determined using eq 5 were similar to those obtained using eq 3.

Product Inhibition Studies. Product inhibition data for the reactions using HIc or isocitrate as the substrate in the direction of α-Ka formation are summarized in Table 2. In the HIc reaction, NADH is NC versus NAD. When the MgHIc concentration is varied, curvature is observed in the double-reciprocal plots in the presence of NADH. At low levels of MgHIc, NADH was competitive versus MgHIc, while at high levels, inhibition became uncompetitive (Figure 5). Data are suggestive of steady state random addition of MgHIc and NAD. α-Ka is UC versus NAD and MgHIc.

Dead-End Inhibition Studies. For the HIc reaction, when isocitrate (slow substrate, Table 1) is used as a dead-end

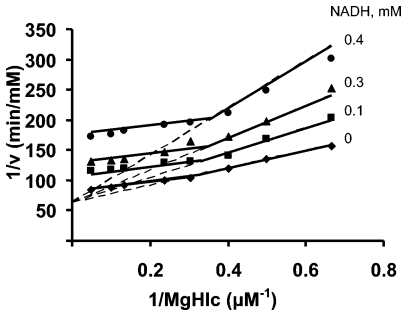

FIGURE 5: Product inhibition by NADH against MgHIc at pH 7.5. The concentration of NAD is fixed at its K_m, and the MgHIc concentration is varied as indicated. Solid lines are a composite obtained from a fit of the data for 1.5−3.3 μM MgHIc to eq 8 and 4.2−21 μM MgHIc to eq 10. Points are experimental values.

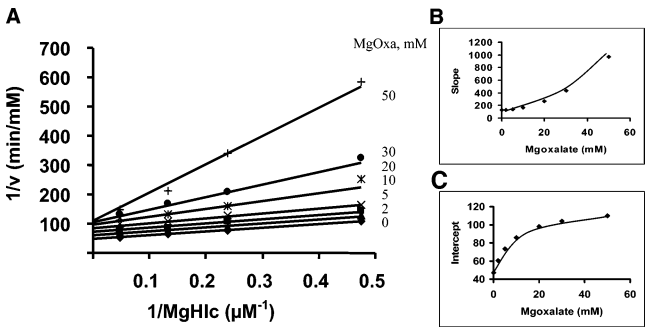

FIGURE 6: S-Parabolic I-hyperbolic noncompetitive inhibition by oxalate against MgHIc. (A) Primary plot exhibiting the S-parabolic I-hyperbolic noncompetitive inhibition by the magnesium oxalate complex vs MgHIc with the NAD concentration fixed at its K_m. (B) Secondary plot of the slope vs oxalate concentration. (C) Secondary plot of the intercept vs oxalate concentration. Rates were measured in 50 mM Hepes (pH 7.5) at 25 °C. The points are experimental or from a graphical analysis, whereas the solid lines are theoretical and based on the kinetic parameters from a fit to eq 11.

inhibitor of HIc, it is C versus MgHIc and NC versus NAD. Citrate, another dead-end analogue of HIc, is also C versus MgHIc and NC versus NAD. Using oxalate as a dead-end inhibitor, a unique inhibition pattern is observed. The secondary slope replot for oxalate inhibition versus MgHIc (Figure 6) or NAD (data not shown) is parabolic, while the intercept replot is hyperbolic, indicating S-parabolic I-hyperbolic NC inhibition (Figure 6).

3-AcPyADP was used as a dead-end analogue of NAD and is C versus NAD. It gave a pattern similar to that inhibited with NADH as a product inhibitor when the MgHIc concentration is varied; i.e., it is C versus MgHIc at low levels of MgHIc but UC at high levels (Figure 7). All dead-end inhibition constants are summarized in Table 3.

For the isocitrate reaction, citrate was chosen as a dead-end analogue of isocitrate and is C versus isocitrate and NC versus NAD. Oxalate, another dead-end inhibitor of isocitrate, is also C versus MgHIc and NC versus NAD. 3-AcPyADP was used as a dead-end analogue of NAD and is C versus NAD and NC versus isocitrate. All dead-end inhibition constants are summarized in Table 4.

Determination of K_{eq} Values. With all reactants, with the exception of α-Ka, fixed as discussed in Materials and Methods, the change in A_{340} (at equilibrium after enzyme was added) was plotted against the α-Ka concentration. The ΔA_{340} is an indicator of displacement from the equilibrium

Table 3: Dead-End Inhibition Patterns for HIcDH with HIc as the Substrate[a]

variable substrate	fixed substrate[b]	inhibitor	K_{is}[c,d] (mM)	K_{ii}[d,e] (mM)	inhibition pattern
MgHIc	NAD	isocitrate	5 ± 1 (5 ± 1)	−	C
NAD	MgHIc	isocitrate	6 ± 1 (1.9 ± 0.3)	7 ± 1 (3.5 ± 0.7)	NC
MgHIc	NAD	citrate	11 ± 2 (11 ± 2)	−	C
NAD	MgHIc	citrate	54 ± 13 (17 ± 3)	85 ± 15 (42 ± 8)	NC
MgHIc (low)	NAD	AcPyADP	5.7 ± 0.5 (1.8 ± 0.3)	−	C
MgHIc (high)	NAD	AcPyADP	−	9.9 ± 0.5 (5.0 ± 0.5)	UC
NAD	MgHIc	AcPyADP	2.5 ± 0.4 (2.5 ± 0.4)	−	C

variable substrate	fixed substrate[b]	inhibitor	K_i[f] (mM)	K_{nom} (mM)	K_{denom} (mM)	inhibition pattern
MgHIc	NAD	oxalate	20 ± 3	9 ± 5	4 ± 1	S-parabolic I-hyperbolic NC
NAD	MgHIc	oxalate	28 ± 2	22 ± 6	6 ± 1	S-parabolic I-hyperbolic NC

[a] Data were obtained at pH 7.5 and 25 °C. [b] Fixed substrates are maintained at their respective K_m. [c] K_{is} represents the inhibition constant for the slope. [d] The values in parentheses are corrected for the fixed substrates where applicable. [e] K_{ii} represents the inhibition constant for the intercept. [f] Average K_i for binding of two molecules of oxalate to the enzyme.

Table 4: Dead-End Inhibition Patterns for HIcDH with Isocitrate as the Substrate[a]

variable substrate	fixed substrate[b]	inhibitor	K_{is}[c,d] (mM)	K_{ii}[d,e] (mM)	inhibition pattern
isocitrate	NAD	citrate	3.8 ± 0.8 (3.8 ± 0.8)	−	C
NAD	isocitrate	citrate	2 ± 1 (1.0 ± 0.4)	1.3 ± 0.4 (0.6 ± 0.1)	NC
isocitrate	NAD	oxalate	3.1 ± 0.2 (3.1 ± 0.2)	−	C
NAD	isocitrate	oxalate	12 ± 4 (6 ± 2)	7 ± 1 (3.5 ± 0.6)	NC
isocitrate	NAD	AcPyADP	1.6 ± 0.5 (0.8 ± 0.3)	6 ± 4 (1.5 ± 0.3)	NC
NAD	isocitrate	AcPyADP	0.64 ± 0.09 (0.55 ± 0.07)	−	C

[a] Data were obtained at pH 7.5 and 25 °C. [b] Fixed substrates are maintained at their respective K_m. [c] K_{is} represents the inhibition constant for the slope. [d] The values in parentheses are corrected for the fixed substrates where applicable. [e] K_{ii} represents the inhibition constant for the intercept.

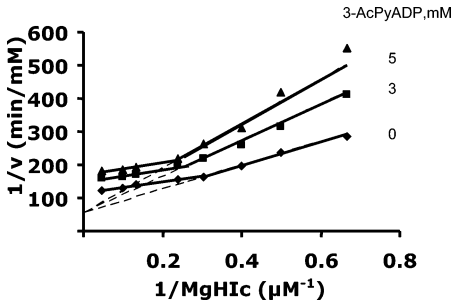

FIGURE 7: Dead-end inhibition by 3-AcPyADP vs MgHIc at pH 7.5. The concentration of NAD is fixed at its K_m, and the MgHIc concentration is varied as indicated. Solid lines are a composite obtained from a fit of the data for 1.5−3.3 μM MgHIc to eq 8 and 4.2−21 μM MgHIc to eq 10. Points are experimental values.

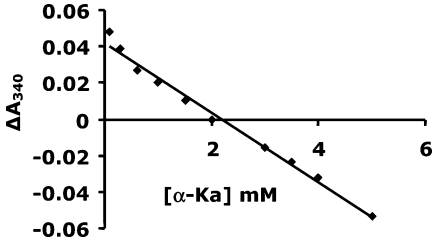

FIGURE 8: Determination of K_{eq} based on the difference in A_{340} vs α-Ka concentration (0.1−5 mM). The points are experimental, while the solid lines are theoretical and based on a fit to the equation for a straight line.

position (Figure 8). The concentration of α-Ka that gave a ΔA_{340} of zero is 2.3 ± 0.1 mM. The K_{eq} calculated using fixed concentrations of the other reactants and 2.3 mM α-Ka (eq 12) is 0.98 M, while the K_{eq} calculated from the Haldane relationship using the kinetic constants given in Table 1 and eq 13 is 0.68 ± 0.03 M.

DISCUSSION

Reaction Catalyzed by HIcDH Using MgHIc as a Substrate. Initial Velocity Studies. An intersecting initial velocity pattern was observed when the initial rate was measured at different concentrations of NAD and different fixed levels of MgHIc, suggesting a sequential kinetic mechanism. The mechanism could be either steady state ordered or random.

In general, for a sequential terreactant mechanism, the initial velocity patterns obtained by varying concentrations of any two substrates with the third fixed at a nonsaturating concentration are all intersecting. If the second substrate to add in an ordered mechanism is fixed at a saturating concentration, the initial velocity pattern obtained by varying the first substrate at a different fixed level of the last becomes parallel (*19*), while three intersecting patterns would be consistent with a fully random mechanism whatever the concentration of the fixed reactant.

In the direction of reductive carboxylation of α-Ka, the data from the systematic analysis were fitted to eq 3 for a fully random terreactant mechanism, where the *B* term in the denominator of the rate equation is not defined, suggesting the EB (E−α-Ka) binary complex is not present. Data are consistent with a fully ordered mechanism or a random one with NADH adding only to free enzyme. Saturation with α-Ka and varying CO_2/NADH gave a parallel pattern. These data are also consistent with the two mechanisms described above.

Interpretation of Product Inhibition Patterns. In the direction of oxidative decarboxylation of HIc, NADH and

Scheme 2. Proposed Kinetic Mechanism for HIcDH with MgHIc as a Substrate

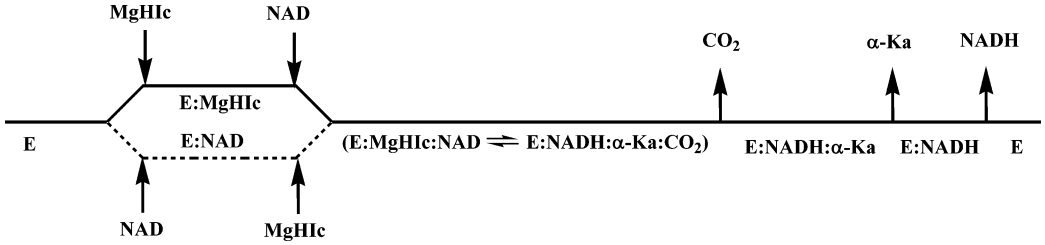

α-Ka were used as product inhibitors. When the MgHIc concentration is varied at a low concentration of NAD (K_m), the NADH inhibition pattern is complex with biphasic double-reciprocal plots (Figure 5) (biphasicity is very slight at zero NADH). At low concentrations of MgHIc, NADH is competitive, likely indicating competition for free enzyme. As the concentration of MgHIc is increased, the pattern becomes uncompetitive, suggesting NADH forms a dead-end complex with E−MgHIc. At low concentrations of MgHIc, free enzyme predominates, while at high concentrations, the E−MgHIc complex is predominant. Data are consistent with switching pathways in a steady state random mechanism. The pathway with MgHIc being added before NAD is slower than that with NAD being added first, and with synergism of binding between the two substrates (*9*). Inhibition by NADH is noncompetitive versus NAD when MgHIc is maintained at a low concentration (K_m). Data are consistent with binding to free enzyme before NAD, which binds with a higher affinity to MgHIc.

α-Ketoadipate is uncompetitive against both MgHIc and NAD, consistent with its release after CO_2 and before NADH. Data are consistent with results of the pairwise analysis; i.e., saturation with α-Ka gave a parallel initial velocity pattern, when the CO_2 and NADH concentrations were varied.

Dead-End Inhibition. 3-Acetylpyridine adenine dinucleotide (3-AcPyADP) was chosen as a dead-end analogue of NAD. It shows competitive inhibition versus NAD and a complex pattern versus MgHIc similar to one observed with NADH as product inhibition (Figure 7). At low concentrations of MgHIc, there is competition between MgHIc and 3-AcPyADP for free enzyme, but as the concentration of MgHIc is increased, most of the enzyme is present as the E−MgHIc enzyme and 3-AcPyADP becomes an uncompetitive inhibitor.

Isocitrate, a dead-end analogue of HIc, is competitive versus MgHIc with NAD at its K_m, while when the NAD concentration is varied, isocitrate is noncompetitive. This indicates either that isocitrate binds to free enzyme and NAD does not or that isocitrate binds to free enzyme competing with NAD and also binds to the E−NAD complex. The latter explanation is also consistent with the proposed random mechanism. Citrate, another dead-end inhibitor of HIc, gave qualitative data identical to those with isocitrate as the inhibitor.

Using oxalate as a dead-end inhibitor, an inhibition pattern is obtained that differs from the others. The secondary slope replot for oxalate inhibition versus MgHIc and NAD is parabolic, while the intercept replot is hyperbolic. The parabolic slope effect indicates the formation of an $E-(Oxa)_2$ complex; i.e., two oxalate molecules bind to free enzyme for inhibition to be observed. The second molecule has a tighter binding than the first one and traps the first molecule on the enzyme. This is a reasonable result, since each of the small oxalate molecules mimics part of the HIc structure, likely binding to the carboxylate binding sites. The intercept effect observed with either the MgHIc or NAD concentration varied likely reflects binding to the E−NADH complex. The hyperbolic intercept effect indicates oxalate cannot trap NADH on the enzyme and NADH can be released at a lower rate for the E−NADH−oxalate complex than for the E−NADH complex. Data thus suggest either there is some randomness on the product site with α-Ka able to bind to E or the small oxalate can bind to the enzyme whether NADH is bound. The rate constant for V at an infinite oxalate concentration will be $V_1(K_{idenum})/(K_{inum})$ which must be ~3-fold lower than V_1 (Table 3 and Figure 6). The complex oxalate inhibition is only observed in the fast reaction direction, since the system is rapid equilibrium in the opposite direction.

An overall kinetic mechanism using MgHIc as a substrate can be proposed and is shown in Scheme 2. On the basis of this mechanism, the rate equation in the direction of HIc formation (eq 4) can be defined in terms of kinetic constants as shown in eq 14.

$$v = \frac{ABC}{K_{ia}K_bK_c + K_{ib}K_cA + 0.2C + K_bAC + K_aBC + K_cAB + ABC} \quad (14)$$

A refit of all initial velocity data using eq 14 gave a K_{ia} value of 0.0047 ± 0.003 mM, a K_{ib} value of 1.7 ± 0.2 mM, and a K_{ic} value is 2.2 ± 0.1 mM. All other constants are given in Table 1.

Kinetic Mechanism of HIcDH Using Isocitrate as the Substrate. The kinetic mechanism with isocitrate, a slow substrate for HIcDH, was studied to compare to that suggested with HIc as the substrate. Slow substrates can simplify the kinetic mechanism as a result of a decrease in the rate of the catalytic portion of the mechanism. Intersecting initial velocity patterns were obtained in the direction of oxidative decarboxylation using isocitrate as a substrate. In this case, the uncomplexed species (Mg^{2+} and isocitrate) bind to the enzyme, unlike the situation with MgHIc. When the data from the systematic analysis were fitted to eq 3 for a fully random terreactant mechanism, the K_c term is not defined, which suggests the addition of Mg^{2+} in rapid equilibrium. Saturation with NAD and varying isocitrate/Mg^{2+} concentrations gave a pattern that intersected on the ordinate, suggesting equilibrium ordered addition of Mg^{2+} prior to isocitrate. A parallel pattern was observed for Mg^{2+}/NAD at a saturating concentration of isocitrate (Figure 4). Since Mg^{2+} adds in a rapid equilibrium prior to isocitrate, the pattern is derived from isocitrate trapping Mg^{2+} on the

Scheme 3. Proposed Kinetic Mechanism for HIcDH with Isocitrate as a Substrate[a]

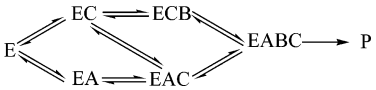

[a] A, B, and C are NAD, isocitrate, and Mg^{2+}, respectively.

enzyme prior to NAD binding. Data suggest ordered binding of Mg^{2+} followed by isocitrate, but with random addition of NAD.

Citrate, oxalate, and 3-AcPyADP were chosen as dead-end analogues of isocitrate and NAD. Citrate exhibits competitive inhibition versus isocitrate, indicating that it binds to the isocitrate binding site. It is a noncompetitive inhibitor versus NAD, indicating that it binds to the E−Mg and E−Mg−NAD enzyme forms. Oxalate gives the patterns qualitatively identical to those obtained with citrate. The hyperbolic intercept effect is eliminated since none of the E−NADH complex builds up in the steady state. The parabolic slope effect with the isocitrate concentration varied is not seen, suggesting only one molecule of oxalate binds to the E or E−NAD complex. Competitive inhibition by 3-AcPyADP versus NAD suggests that it binds to the same enzyme forms as NAD. The noncompetitive inhibition versus isocitrate indicates that it binds to the E−Mg and E−Mg−isocitrate complex. These dead-end inhibition patterns are consistent with the proposed random mechanism shown in Scheme 3. Indeed, use of the slow substrate simplified the analysis, and the mechanism was reduced to one that at least approximates rapid equilibrium random, not surprising given the >200-fold decrease in V/E_t for isocitrate compared to MgHIc.

For dead-end inhibitors, the measured appK_i values must be corrected for the fixed reactant concentrations to give the true K_i value. The dead-end inhibition data were quantitatively analyzed according to the method of ref *20*.

Although isocitrate and HIc have a very similar structure, the chelate complex, MgHIc, is the form that binds to the enzyme, similar to Mg isocitrate for ICDH (*21*). However, uncomplexed isocitrate and metal ion are substrates for HIcDH. The kinetic mechanism for both substrates is random in the forward reaction direction. The larger K_m value and lower k_{cat} value with isocitrate as the substrate are consistent with HIcDH being specific for HIc.

ACKNOWLEDGMENT

We thank Dr. Lei Li for help with subcloning the gene for HIcDH. We thank Dr. David R. J. Palmer for supplying homoisocitrate.

REFERENCES

1. Strassman, M., and Ceci, L. N. (1965) Enzymatic Formation of α-Ketoadipate Acid from Homoisocitric Acid, *J. Biol. Chem. 240*, 4357−4361.
2. Zabriskie, T. M., and Jackson, M. D. (2000) Lysine Biosynthesis and Metabolism in Fungi, *Nat. Prod. Rep. 17*, 85−97.
3. Garrad, R. C., and Bhattacharjee, J. K. (1992) Lysine Biosynthesis in Selected Pathogenic Fungi: Characterization of Lysine Auxotrophs and the Cloned LYS 1 Gene of *Candida albicans*, *J. Bacteriol. 174*, 7379−7384.
4. Andi, B., West, A. H., and Cook, P. F. (2004) Stabilization and Characterization of Histidine-tagged Homocitrate Synthase from *Saccharomyces cerevisiae*, *Arch. Biochem. Biophys. 421*, 243−254.
5. Johansson, E., Steffens, J. J., Lindqvist, Y., and Schneider, G. (2000) Crystal Structure of Saccharopine Reductase from *Magnaporthe grisea*, an Enzyme of the α-Aminoadipate Pathway of Lysine Biosynthesis, *Structure 8*, 1037−1047.
6. Karsten, W. E., and Cook, P. F. (2000) Pyridine Nucleotide-dependent β-Hydroxyacid Oxidative Decarboxylases: An Overview, *Protein Pept. Lett. 7*, 281−286.
7. Cohen, P. F., and Colman, R. F. (1974) Role of Manganous Ion in the Kinetics of Pig-Heart NAD-Specific Isocitrate Dehydrogenase, *Eur. J. Biochem. 47*, 35−45.
8. Dean, A. M., and Dvorak, L. (1995) The Role of Glutamate 87 in the Kinetic Mechanism of *Thermus thermophilus* Isopropylmalate Dehydrogenase, *Protein Sci. 4*, 2156−2167.
9. Park, S. H., Kiick, D. M., Harris, B. G., and Cook, P. F. (1984) Kinetic Mechanism in the Direction of Oxidative Decarboxylation for NAD-malic Enzyme from *Ascaris suum*, *Biochemistry 23*, 5446−5454.
10. Mallick, S., Harris, B. G., and Cook, P. F. (1991) Kinetic Mechanism of NAD-malic Enzyme from *Ascaris suum* in the Direction of Reductive Carboxylation, *J. Biol. Chem. 266*, 2732−2738.
11. Weiss, P. M., Gavva, S. R., Harris, B. G., Urbauer, J. F., Cleland, W. W., and Cook, P. F. (1991) Multiple Isotope Effects with Alternative Dinucleotide Substrates as a Probe of the Malic Enzyme Reaction, *Biochemistry 30*, 5755−5763.
12. Uhr, M. L., Thompson, V. W., and Cleland, W. W. (1974) The Kinetics of Pig Heart Triphosphopyridine Nucleotide-Isocitrate Dehydrogenase. I. Initial Velocity, Substrate and Product Inhibition, and Isotope Exchange Studies, *J. Biol. Chem. 249*, 2920−2927.
13. Northrop, D. B., and Cleland, W. W. (1974) The Kinetics of Pig Heart Triphosphopyridine Nucleotide-Isocitrate Dehydrogenase. II. Dead-end and Multiple Inhibition Studies, *J. Biol. Chem. 249*, 2928−2931.
14. Dean, A. M., and Koshland, D. E. (1993) Kinetic Mechanism of *Escherichia coli* Isocitrate Dehydrogenase, *Biochemistry 32*, 9302−9309.
15. Berdis, A. J., and Cook, P. F. (1993) Overall Kinetic Mechanism of 6-Phosphogluconate Dehydrogenase from *Candida utilis*, *Biochemistry 32*, 2036−2040.
16. Price, N. E., and Cook, P. F. (1996) Kinetic and Chemical Mechanism of the Sheep Liver 6-Phosphogluconate Dehydrogenase, *Arch. Biochem. Biophys. 336*, 215−223.
17. Tipton, P. (1993) Intermediate Partitioning in the Tartrate Dehydrogenase-Catalyzed Oxidative Decarboxylation of D-malate, *Biochemistry 32*, 2822−2827.
18. Nelson, R. B., and Gribble, G. W. (1973) On the Preparation of α-Ketoadipic Acid, *Org. Prep. Proced. Int. 5*, 55−58.
19. Cleland, W. W. (1970) Steady-state Enzyme Kinetics, in *The Enzymes* (Boyer, P. D., Ed.) Vol. 2, pp 1−65, Academic Press, New York.
20. Xu, H., West, A. H., and Cook, P. F. (2006) Overall Kinetic Mechanism of *Saccharopine dehydrogenase* from *Saccharomyces cerevisiae*, *Biochemistry 45*, 12156−12166.
21. Willson, V. J. C., and Tipton, K. F. (1981) The Activation of Ox-Brain NAD^+-dependent Isocitrate Dehydrogenase by Magnesium Ion, *Eur. J. Biochem. 113*, 477−483.

BI062067Q